Charge-Density-Wave Mechanism in 2H-NbSe₂: Photoemission Results

Th. Straub,[1] Th. Finteis,[1] R. Claessen,[1,2,*] P. Steiner,[1] S. Hüfner,[1] P. Blaha,[3] C. S. Oglesby,[4] and E. Bucher[5]

[1]*Fachrichtung Experimentalphysik, Universität des Saarlandes, D-66041 Saarbrücken, Germany*
[2]*Experimentalphysik II, Universität Augsburg, D-86135 Augsburg, Germany*
[3]*Institut für Technische Elektrochemie, Technische Universität Wien, A-1060 Wien, Austria*
[4]*Lucent Technologies, Murray Hill, New Jersey 07974*
[5]*Fakultät für Physik, Universität Konstanz, D-78434 Konstanz, Germany*
(Received 13 October 1998)

The layered charge-density-wave (CDW) material 2H-NbSe₂ was studied by angle-resolved photoelectron spectroscopy. We present the first experimental mapping of the Fermi surface (FS) portions involved in the CDW transition. From this and additional data on the conduction band dispersion near the Fermi level we conclude that the CDW instability in this material is driven by FS nesting and not by saddle point singularities. [S0031-9007(99)09298-4]

Among the many transition metal dichalcogenides (TMDCs) with charge-density-wave (CDW) instabilities, 2H-NbSe₂ is a particularly interesting case. It undergoes at $T_{CDW} \approx 35$ K a second-order phase transition into an incommensurate two-dimensional CDW phase [1]. The (threefold degenerate) CDW vectors are oriented along the ΓM directions of the hexagonal Brillouin zone (BZ) and have a magnitude of $|\mathbf{Q}_{CDW}| = \frac{2}{3}|\Gamma M|(1 - \delta) = 0.688$ Å^{-1} [1]. The quantity $\delta \approx 0.02$ is a measure of the incommensurability and is slightly temperature dependent. The resistivity of 2H-NbSe₂ remains metallic below T_{CDW} and shows only a small anomaly at the phase transition, indicating that the CDW does not involve a large modification of the Fermi surface [2]. Upon further cooling, 2H-NbSe₂ finally enters a superconducting phase ($T_c = 7.2$ K) [2,3] which coexists with the CDW [1].

The precise origin of the CDW instability in 2H-NbSe₂ (and other TMDCs of the 2H polytype) has been a matter of debate for years. Some authors argue that the phase transition is driven by Fermi surface (FS) nesting [4,5], with electron-phonon matrix elements playing an additional role [6]. This mechanism is similar to the Peierls instability in one-dimensional metals [7], except that in the quasi-two-dimensional 2H-NbSe₂ only fractions of the FS satisfy the required nesting condition. Because the remaining FS parts do not participate in the transition, the CDW is *not* accompanied by a metal-insulator transition, unlike in one dimension. The CDW vector is given by the nesting vector $\mathbf{Q}_{FS}$. A completely different mechanism has been suggested by Rice and Scott [8]. They have shown that a two-dimensional conduction band with saddle points close to the Fermi level is unstable against CDW formation. In this theory the CDW vector is determined by the **k**-space separation $\mathbf{Q}_{SP}$ between two saddle points, with the relevant pair of saddle points depending in addition on the electron-phonon coupling strength. Both CDW theories are based on band theoretical results [9,10] on conduction band dispersion and Fermi surface topology. Experimental information is, however, scarce, in particular, because

the relevant FS sheets have never been observed in de Haas–van Alphen (dHvA) experiments [11–14]. A very recent high-resolution photoemission study on the related compound 2H-TaSe₂ confirmed an extended saddle band region near the Fermi energy [15]. Large CDW-induced energy shifts observed in this region seem to favor the Rice-Scott mechanism for this material.

In this Letter we report on angle-resolved photoemission spectroscopy (ARPES) on 2H-NbSe₂. We have performed a direct mapping of the Fermi surface sheets responsible for the CDW formation and find that they display nesting behavior in good agreement with the observed CDW vector. From energy distribution curves we confirm the existence of saddle points near the Fermi level. Their position, however, cannot account for the actual CDW periodicity.

The ARPES experiments were performed mainly with a VG ESCALAB Mk. 2 spectrometer equipped with a two-axis manipulator, which allows photoelectron detection over the entire half-space above the sample surface [16]. The spectra were measured with He-I radiation (21.2 eV) at room temperature, employing energy and angular resolutions of 60 meV and 1.5°, respectively, except where otherwise stated. Clean (0001) surfaces were prepared by *in situ* cleavage of the 2H-NbSe₂ crystals.

Fermi surface. — The FS topology in 2H-NbSe₂ is intimately related to its layered crystal structure. Early non-self-consistent band calculations [9,10] found that the predominantly Nb 4d-derived conduction band displays an almost two-dimensional dispersion, thus leading to two sets of cylindrical hole surfaces centered about the ΓA and KH lines of the BZ, respectively [10]. Because the unit cell of the 2H polytype contains two formula units, all bands and hence FS sheets are actually doubled. Their degeneracy is slightly lifted by interlayer coupling and spin-orbit interaction. The interlayer interaction also causes a small corrugation of the cylinders along the k_z direction. More recent density-functional calculations [13,17] including our own [18] yield an additional small pancake-

shaped hole surface centered at the Γ point. It originates from a k_z-dispersive band of mostly Se $4p_z$ origin.

While dHvA measurements have confirmed the pancake object, no dHvA signal has ever been observed for the cylindrical FS sheets [11–14]. It has been speculated [12,13] that the formation of large electron orbits around the cylinders is prevented by the incommensurability of the CDW, which is always present at the low temperatures required for dHvA measurements. The only experimental evidence so far for the existence of cylindrical FS sheets comes from electron-positron annihilation, which finds a hole cylinder aligned along ΓA but still fails to detect the one along KH [19].

In Fig. 1 we display our ARPES results on the Fermi surface. Figure 1(a) contains the photoelectron intensity distribution $I(\mathbf{k}_\parallel, E_F)$ excited from the Fermi level E_F. Here $\mathbf{k}_\parallel$ denotes the surface-projected photoelectron wave vector. The intensity distribution thus represents an image of the two-dimensional FS cross section [20–22]. As predicted by band theory, the map shows a FS of hexagonal shape in the BZ center and a second sheet centered about $K(H)$, which is observed here for the first time. At the outer edge of the map, one can even see parts of the ΓA cylinder(s) in the next BZ. The double-walled nature of the FS sheets is not resolved. The intensity bridges between the ΓA and KH surfaces seen along the $\Gamma K(AH)$ direction result from the low binding energy of the conduction band, which in this region is smaller than the width of the resolution-limited energy detection window (see below). No indication is observed for the Γ-centered flat pancake surface. Because of its small k_z extension, it is probably not accessible by He-I radiation [23].

Obviously, the hexagonal shape of the inner hole cylinder provides ideal nesting conditions, with the nesting vector $\mathbf{Q}_{FS}$ given by the edge-to-edge distance along ΓM. For a more detailed view of the inner FS we display in Fig. 1(b) the modulus of the two-dimensional intensity gradient $|\nabla_{\mathbf{k}_\parallel} I|$. In many cases the gradient map allows a more accurate estimate of FS contours than the original intensity distribution [22]. However, this method can fail, if the linewidth of the ARPES peak responsible for the FS signal exceeds that of the energy detection window [16]. In this case Fermi vector locations may still be better obtained from the intensity maxima. The two conduction bands making up the cylindrical FS sheets in $2H$-NbSe$_2$ behave differently in that respect. Though not resolved in the FS maps of Fig. 1, they are distinguishable in the energy distribution curves of Fig. 2. Whereas the peak at higher binding energy displays a linewidth of $\sim$200 meV, much larger than the instrumental resolution, the very shallow dispersion of the near-E_F structure prevents a reliable estimate of its width; it may be comparable to the energy window. This makes it difficult to define a unique criterion for a correct FS determination. Nonetheless, the intensity and gradient maps still provide upper and lower bounds, respectively, for the nesting vector of the ΓA cylinder. From
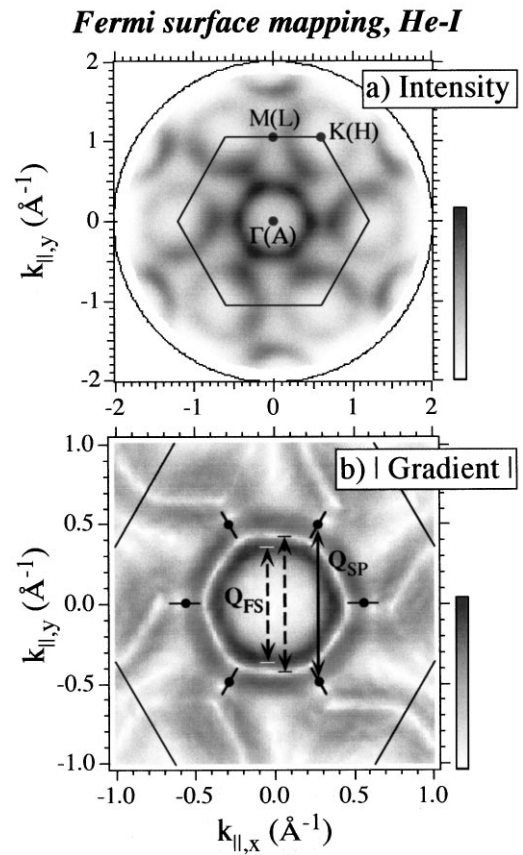

FIG. 1. Fermi surface mapping of $2H$-NbSe$_2$ by ARPES (angular resolution: $\pm 1.75°$): (a) photoelectron intensity distribution versus in-plane momentum $\mathbf{k}_\parallel$. Also shown is the Brillouin zone with its critical points. (b) Modulus of the two-dimensional intensity gradient on an enlarged $\mathbf{k}_\parallel$-scale. The position of the conduction band saddle points is marked by solid circles (including error bars); the vector $\mathbf{Q}_{SP}$ connects two saddle points along the ΓM azimuth. The dashed arrows denote the upper and lower limits of the Fermi surface nesting vector $\mathbf{Q}_{FS}$ (see text).

the contours of maximum intensity in Fig. 1(a), or equivalently the contour of zero gradient in Fig. 1(b) (white contour), we obtain an upper limit of $\mathbf{Q}_{FS} \leq 0.87$ Å^{-1}. The lower limit is derived from the intense inner contour (i.e., the one next to the unoccupied region around $\Gamma(A)$ [22]) in the gradient map: $\mathbf{Q}_{FS} \geq 0.69$ Å^{-1}. Because of the blurred appearance of the KH cylinders in the intensity map and the discussed problem of correct FS data interpretation, we are reluctant to extract equally detailed information for the ΓA cylinder.

Saddle points.—Calculations predict two-dimensional saddle point behavior in the conduction band dispersion about half-way along ΓK [9,10,13,17,18]. Rice and Scott have shown that the (sixfold degenerate) saddle point can lead to a CDW instability, if it lies close enough to the Fermi level, i.e., if its binding energy is comparable to $k_B T_{CDW}$ ($\approx$3 meV in $2H$-NbSe$_2$). However, in the band theory the saddle point appears at a much higher energy ($\sim$200 meV). In addition, the calculated distance between a pair of saddle points (measured parallel to the
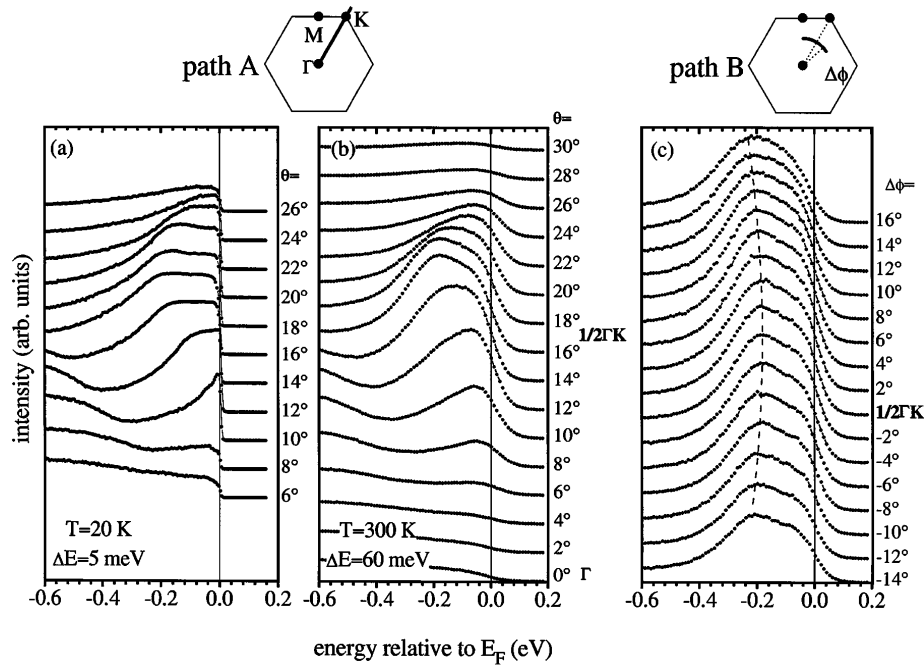
FIG. 2. Energy distribution curves on the dispersion of the Nb $4d$-like conduction band doublet along $\Gamma K(AH)$ (path A) [(a) and (b)] and along a circular trajectory with fixed $|\mathbf{k}_\parallel| = \frac{1}{2}\Gamma K$ (path B) (c). The EDCs in (a) are high-resolution data measured at 20 K [24]. The dashed curve in (c) serves as guide to the eye.

ΓM direction) would lead to an incorrect 2×2 CDW superstructure [4,10].

In order to obtain experimental information on the saddle points we have measured energy distribution curves (EDCs) in the relevant **k**-space region. Figure 2(b) shows a room-temperature series of EDCs measured along the $\Gamma K(AH)$ azimuth ("path A"); some additional high-resolution spectra taken at 20 K [24] are contained in Fig. 2(a). In both data sets the conduction band emission appears at an emission angle of $\theta = 10°$ and disappears again for $\theta > 24°$. The highest binding energy, i.e., the dispersion *minimum*, is assumed at about $\frac{1}{2}\Gamma K$, where the spectra display a distinct double structure. Except for a sharpening of the Fermi edge, the 20 K spectra show the same behavior as the room-temperature data and, in particular, no indication of a CDW-induced gap opening. Figure 2(c) displays EDCs measured on a circular trajectory with fixed in-plane momentum $|\mathbf{k}_\parallel| = \frac{1}{2}\Gamma K$ but varying azimuthal angle $\Delta\phi$ off the $\Gamma K(AH)$ line ("path B"). The higher binding energy ($\sim$200 meV) peak of the doublet shows a small but detectable downward dispersion for increasing $|\Delta\phi|$, i.e., $\Delta\phi = 0$ corresponds to a dispersion *maximum*. This verifies that at least the deeper lying conduction band has a saddle point near $\frac{1}{2}\Gamma K(AH)$.

However, for a possible role in the CDW instability, the band closer to the Fermi level is of greater importance. In the high-resolution spectra of Fig. 2(a) it appears as a weak emission riding on the low binding energy tail of the much broader 200 meV peak and cut off by the extremely sharp Fermi edge at 20 K, thereby giving rise to a peculiar double-peak line shape. In the room-temperature

spectra [Fig. 2(b)] the near-E_F "peak" degenerates into a shoulder. While it is difficult to derive a precise binding energy for this feature, it certainly does not exceed 50 meV. The lower binding energy conduction band thus appears strongly renormalized relative to band theory. A similar observation has recently been made for $2H$-TaSe$_2$ [15].

The saddle point location in reciprocal space was determined from the room-temperature spectra (due to instrumental limitations, high-resolution data could not be taken along nonazimuthal directions [24]). Figure 3 displays the negative second derivative $-\frac{\partial^2}{\partial E^2} I(k_\parallel, E)$ of the EDCs in Figs. 2(a) and 2(b) as gray-scale maps, cut off below a suitable threshold to suppress noise and negative values [25]. Away from the Fermi level this quantity yields a good estimate of the actual peak energy, but like the intensity gets strongly distorted near E_F, when thermal and instrumental broadening is large. Nonetheless, as the energy of a maximum in $-\frac{\partial^2}{\partial E^2} I(k_\parallel, E)$ is a monotonous function of the true binding energy, it still contains information on the qualitative band dispersion and, in particular, *the character of the band extrema*. The plots in Fig. 3 thus correctly reflect the band minima and maxima of the two conduction bands along paths A and B, respectively, though they cannot account truthfully for absolute binding energies close to E_F. For comparison, we also display our calculated conduction bands [18]. From the data in Fig. 3 we locate the saddle point of the near-E_F band at 0.56 ± 0.09 Å^{-1} along ΓK ($= 46\% \pm 7\%$ ΓK). Its position is also marked in the gradient map of Fig. 1(b), agreeing well with the location of zero gradient (white spots), as it should.
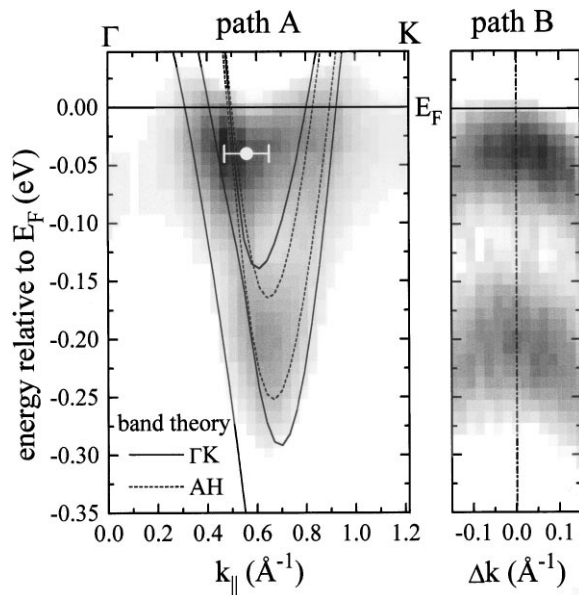
FIG. 3. Negative second derivative of the EDCs in Fig. 2 as a clipped gray-scale plot (see text for details). The saddle point of the upper band is marked by the solid white circle. Also included are our density-functional bands along ΓK and AH. Note that near the Fermi level the maxima in $-\frac{\partial^2}{\partial E^2} I(k_\parallel, E)$ reflect only the qualitative dispersion and should not be confused with the true binding energies.

Conclusions. — Our ARPES data not only verify the existence of a saddle point at $\sim \frac{1}{2}\Gamma K$ but also find the Fermi vectors along $\Gamma K(AH)$ in good correspondence with band theory (cf. Fig. 3). These findings differ from the ARPES results of Liu *et al.* [15] on $2H$-TaSe$_2$, which show an *extended* saddle band, with the occupied range along $\Gamma K(AH)$ much wider than predicted by band calculations. In agreement with Ref. [15], our data indicate that the near-E_F band lies much closer to the Fermi level than predicted by both the earlier band calculations as well as our density-functional result. This suggests strong band renormalization due to electron-electron or electron-phonon interaction. The **k**-space location of the saddle point is not consistent with the Rice-Scott model: The resulting separation between the relevant pair of saddle points [cf. Fig. 1(b)] is $|\mathbf{Q}_{SP}| = 0.97 \pm 0.16$ Å^{-1}, far off the observed $|\mathbf{Q}_{CDW}| = 0.688$ Å^{-1}. This finding and the apparent absence of a gap opening in the 20 K spectra (i.e., below T_{CDW}) around the saddle point [Fig. 2(a)] give experimental support to earlier suppositions [4,10] that the CDW instability in $2H$-NbSe$_2$ is not explained by the Rice-Scott mechanism. For $2H$-TaSe$_2$, Liu *et al.* arrived at a different conclusion [15].

The data in Fig. 1 rather suggest that the CDW transition in $2H$-NbSe$_2$ is driven by FS nesting. This not only leads to the hexagonal cross section of the ΓA-centered hole cylinder almost perfect (self-)nesting of the correct orientation but also the size of the corresponding nesting vector, $|\mathbf{Q}_{FS}| = 0.69 - 0.87$ Å^{-1}, from our conservative estimate, is reasonably close to the observed CDW

vector. A slight deviation of $\mathbf{Q}_{CDW}$ from the bare nesting vector could be caused by electron-phonon matrix elements or additional contributions from intersheet nesting, if this maximizes the CDW energy gain.

*Corresponding author.
Electronic address: claessen@physik.uni-augsburg.de

[1] D. E. Moncton, J. D. Axe, and F. J. DiSalvo, Phys. Rev. Lett. **34**, 734 (1975).
[2] J. M. E. Harper, T. H. Geballe, and F. J. DiSalvo, Phys. Lett. **54A**, 27 (1975).
[3] E. Revolinski, B. E. Brown, D. Beerntsen, and C. H. Armitage, J. Less-Common Met. **8**, 63 (1965).
[4] J. A. Wilson, Phys. Rev. B **15**, 5748 (1977).
[5] N. J. Doran *et al.*, J. Phys. C **11**, 699 (1978).
[6] N. J. Doran, J. Phys. C **11**, L959 (1978).
[7] G. Grüner, Rev. Mod. Phys. **60**, 1129 (1988).
[8] T. M. Rice and G. K. Scott, Phys. Rev. Lett. **35**, 120 (1975).
[9] L. F. Mattheiss, Phys. Rev. B **8**, 3719 (1973).
[10] G. Wexler and A. M. Woolley, J. Phys. C **9**, 1185 (1976).
[11] J. E. Graebner and M. Robbins, Phys. Rev. Lett. **36**, 422 (1976).
[12] Y. Onuki *et al.*, J. Phys. Soc. Jpn. **61**, 692 (1992).
[13] R. Corcoran *et al.*, J. Phys. Condens. Matter **6**, 4479 (1994).
[14] E. Steep *et al.*, Physica (Amsterdam) **204B**, 162 (1995).
[15] R. Liu, C. G. Olson, W. C. Tonjes, and R. F. Frindt, Phys. Rev. Lett. **80**, 5762 (1998).
[16] Th. Straub, Ph.D. thesis, Universität des Saarlandes, 1998.
[17] V. Eyert (private communication).
[18] Our density-functional band structure was obtained by a relativistic full-potential linearized augmented plane wave calculation based on the local density approximation, using the WIEN97 code by P. Blaha, K. Schwarz, and J. Luitz (Technische Universität Wien, 1997).
[19] K. Takita *et al.*, Physica (Amsterdam) **185C–189C**, 2717 (1991).
[20] A. Santoni, L. J. Terminello, F. J. Himpsel, and T. Takahashi, Appl. Phys. A **52**, 299 (1991).
[21] P. Aebi *et al.*, Phys. Rev. Lett. **72**, 2757 (1994).
[22] Th. Straub *et al.*, Phys. Rev. B **55**, 13 473 (1997).
[23] This is inferred from normal emission spectra measured with variable photon energy. R. Claessen *et al.* (unpublished).
[24] These spectra were taken with a Scienta 200 analyzer, employing energy and angular resolutions of 5 meV and 0.3°, respectively. They were reproduced on two samples. Because the experimental setup does not allow a rotation of the sample, EDCs could only be measured along the ΓK azimuth and no FS mapping could be performed. We note, however, that the one-dimensional photoelectron distribution $I(\mathbf{k}_\parallel, E_F)$ extracted from the ΓK EDCs is consistent with the data of Fig. 1.
[25] V. N. Strocov *et al.*, Phys. Rev. Lett. **81**, 4943 (1998).